Figure	Condition	# Male	# Female	Figure	Condition	# Male	# Female
Fig 1a-f	All	7	9	**Fig 7h-i**	All	2	4
Fig 1h-j	All	3	5	**Fig 7k**	S ND	4	5
Fig 1k,l	All	?	?		S 4MD	8	7
Fig 2a-f	All	4	3		N ND	2	3
Fig 2h	All	3	4		N 4MD	6	3
Fig 2i-k	All	6	4		NC ND	3	2
Fig 2l	Control	6	3		NC 4MD	6	3
Fig 2n	Control	3	1		DSP4 ND	3	2
	Th-Cre	1	3		DSP4 4MD	2	3
Fig 3b	S	3	3	**SFig 1**		?	?
	N	2	3	**SFig 1m**	Control	5	3
	NC	3	3		Trained	4	4
Fig 3d-f	S	2	5		Stressed	4	5
	N	4	4	**SFig 2**		?	?
	NC	3	3	**SFig 3**		?	?
Fig 3h	S	6	10	**SFig 4**	All	2	2
	N	4	4	**SFig 5a-c**	All	3	2
	NC	6	6	**SFig 5d-f**	All	3	4
	DSP4	6	6	**SFig 5g-j**	All	3	4
	ICI	5	6	**SFig 6a**	All	7	9
Fig 4b	NC	3	3	**SFig 6b**	All	4	3
Fig 4b	ICI	4	3	**SFig 7a-f**	All	0	4
Fig 4c,e,h	All	3	3	**SFig 7h-i**	All	3	3
Fig 4i,d,f	All	4	3	**SFig 8b**	S	2	1
Fig 5 a-e	S	2	3		DSP4 2D	3	2
	N	4	3		DSP4 6D	2	2
	NC	2	3	**SFig 9a,b**	S	3	3
	DPS4	2	4		N	2	3
	ICI	2	4		NC	3	3
Fig 6c	S ND	11	4	**SFig 10**		?	?
	S 4MD	8	6	**SFig 11**	S	6	10
	N ND	5	1		N	4	4
	N 4MD	4	2		NC	6	6
	NC ND	2	4		DSP4	6	6
	NC 4MD	5	6		ICI	5	6
	DSP4 ND	4	2	**SFig 12a**	All	3	3
	DSP4 4MD	2	6	**SFig 12b**	All	4	3
Fig 6e	S	2	5	**SFig13 a**	S ND	2	1
	N	0	3		S 4MD	1	2
	NC	0	5		ICI ND	2	1
	DSP4	2	2		ICI 4MD	7	2
Fig 7c	Cre Ai9 S	3	1	**SFig 13b**	S	3	3
	Cre Ai9 NC	0	4		ICI	2	1
	CreB2 Ai9 S	2	3	**SFig 14f,g**	CreB2	1	2
	CreB2 Ai9 NC	4	1		CreB2+Tam	0	3
Fig 7d-f	All	2	2	**SFig 14i**	CreB2	3	5
Fig 7g	S ND	5	5		CreB2+Tam	1	4
	S 4MD	5	4				
	N ND	1	3				
	N 4MD	4	1				
	NC ND	2	4				
	NC 4MD	3	7				
	DSP4 ND	1	5				
	DSP4 4MD	5	2				

Supplementary Table 1| Sex distribution for all experiments.

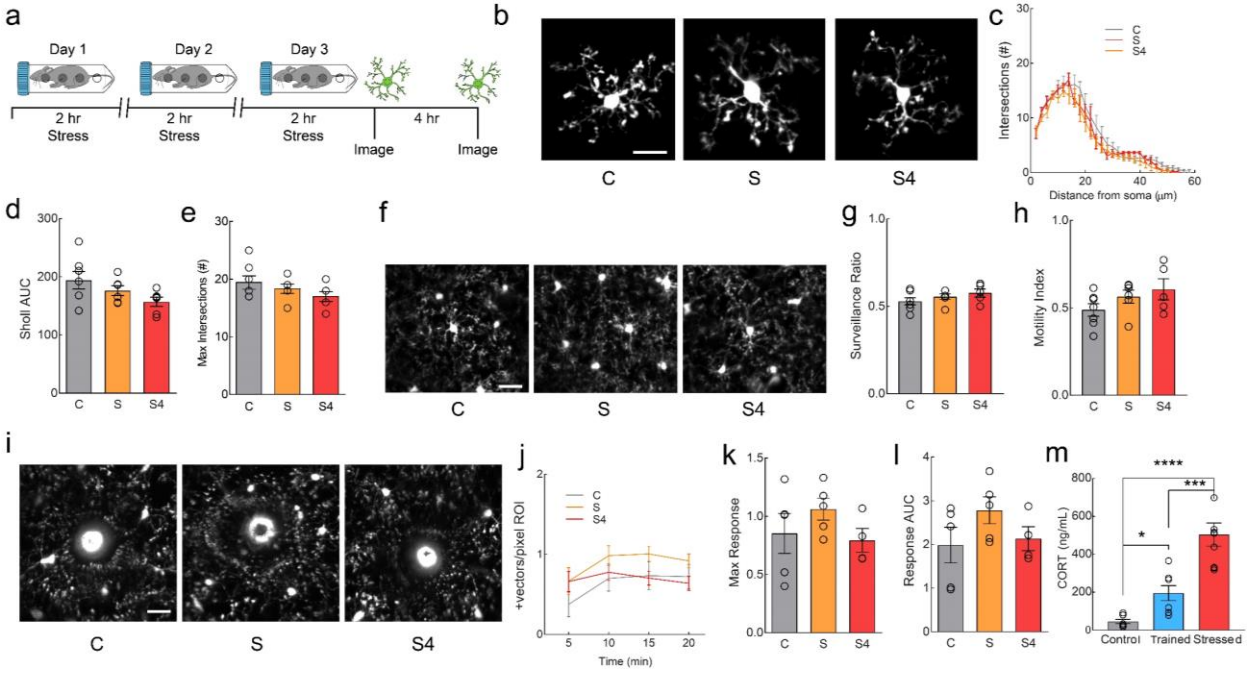

Supplementary Figure 1| Acute stress does not affect microglial morphology, motility, or injury response. (**a**) Schematic of the stress paradigm. Mice were restrained in a translucent tube under bright light for 2 hours daily for three days before imaging under fentanyl anesthesia. Control mice (C) were handled, but were returned to their cage prior to imaging. Microglia in stressed mice were imaged immediately following the last restraint period (S) or 4 hours later (S4). (**b**) Example microglia for control (C), stressed (S) or stressed post 4 hour (S4) mice. (**c**) Sholl analysis demonstrating no difference in number of intersections as a function of distance from soma across all conditions (n: C=7, S=6, S4=6 mice, 3-5 microglia per animal). (**d**) Sholl area under curve (AUC) showing no significant difference with stress (n: C=7, S=6, S4=6 mice, one-way ANOVA, p=0.10, F(2,16)=2.63). (**e**) The maximum number of Sholl intersections was also not significantly different between all conditions (n: C=7, S=6, S4=6 mice, one-way ANOVA, p=0.24, F(2,16)=0.49). (**f**) Example 2D max-projection images of surveillance over a 30 minute period for control, stress and stress +4hrs conditions. (**g**) The surveillance ratio was not significantly different between all conditions (n: C=7, S=6, S4=5 mice, one-way ANOVA, p=0.28, F(2,15)=1.39). (**h**) No significant difference in motility index was found across all conditions (n: C=7, S=6, S4=5 mice, one-way ANOVA, p=0.18, F(2,15)=1.91). (**i**) Example microglial responses to laser ablation after 30 minutes in each condition. (**j**) Graph of the response vectors as a function of time (n: C=5, S=5, S4=4 mice). (**k**) No significant difference was observed for the maximum response vector (n: C=5, S=5, S4=4 mice, one-way ANOVA, p=0.35, F(2,11)=1.15). (**l**) Area under curve (AUC) was not significantly different (n: C=5, S=5, S4=4 mice, one-way ANOVA, p=0.25, F(2,11)=1.58). (**m**) Restraint stress produced significantly elevated levels of corticosterone when compared to both control naïve animals as well as those trained for imaging as measured by a corticosterone ELISA (n: control=8, trained=8, stressed=9 mice, one-way ANOVA, $p=8.4x10^{-7}$, F(2,22)=28.24, Holm-sidak multiple comparisons, control v. trained p=0.030, control v. stressed $p=7.4x10^{-7}$, trained v. stressed p=0.00012). Scale bar = 25µm. Graphs show mean±SEM; *p<0.05, **p<0.01, ***p<0.005, ****p<0.0001. Points represent individual animals. See Supplementary Table 1 for the number of females and males used in these experiments.

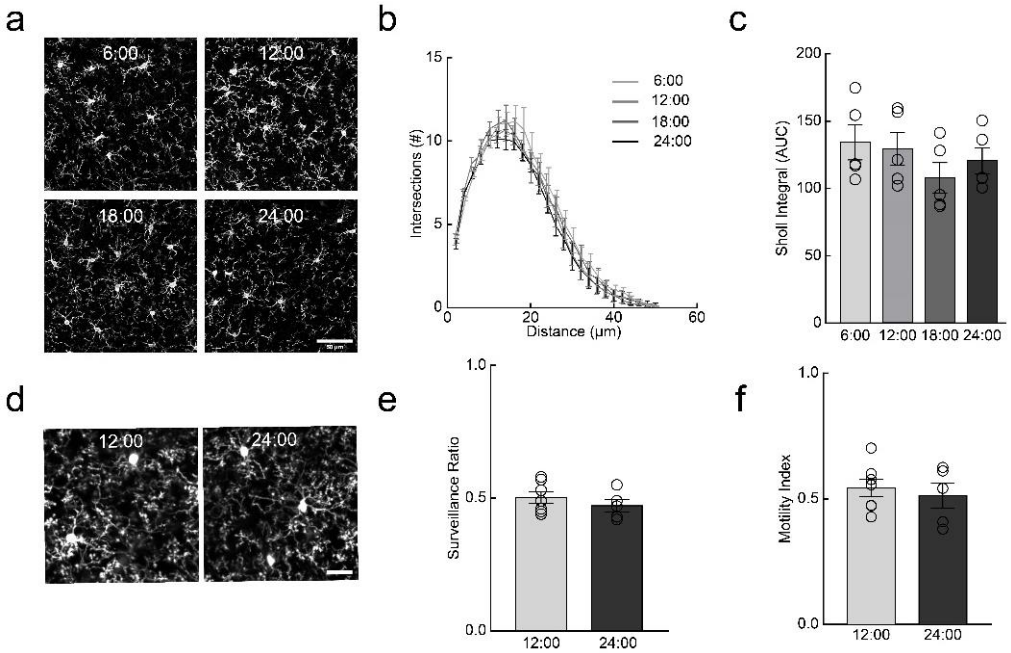

Supplementary Figure 2| Circadian rhythm does not affect microglial morphology or dynamics in anesthetized animals. (**a**) Example images of microglial morphology in fixed tissue stained for the microglial marker, Iba-1. Animals were sacrificed at four time points through the dark/light cycle corresponding to zeitgeber 6, 12, 18 and 24 (Scale bar = 50µm). (**b**) Sholl analysis for microglia at each time point (n=5 mice/group, 15 microglia per animal). (**c**) No difference was found for the Sholl integral (AUC, area under curve, n=5 mice for all groups, one-way ANOVA, p=0.42, F(3,16)=1.00). (**d**) Example 2D max projection of microglial process surveillance over 30 minutes imaged at zeitgeber 12 and 24 (Scale bar = 25µm). (**e**) Quantification of surveillance ratio showed no significant difference between either time point (n: 12:00=7, 24:00=5 mice, two-sided t-test, p=0.36, t(10)=0.95). (**f**) No difference was observed in motility index (n: 12:00=7, 24:00=5 mice, two-sided t-test, p=0.62, t(10)=0.52). The absence of change in any of our parameters of microglial physiology suggests that circadian rhythm does not impact microglial dynamics. Graphs show mean±SEM. Points represent individual animals. See Supplementary Table 1 for the number of females and males used in these experiments.

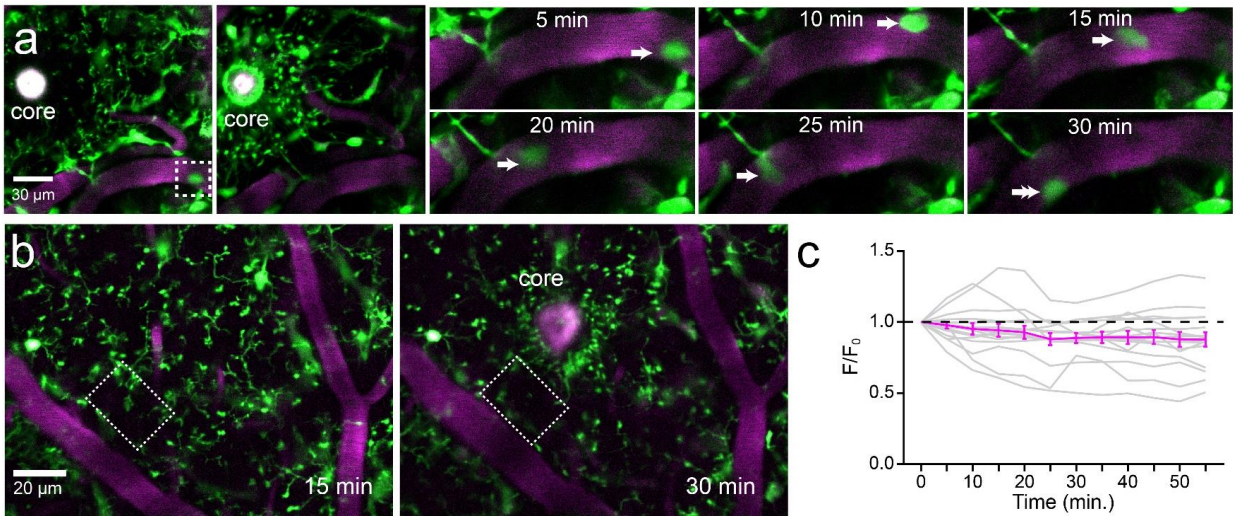

Supplementary Figure 3| Laser ablation does not disrupt the integrity of the blood-brain barrier. (**a**) Time lapse imaging of microglial response to laser ablation (core) and circulating monocyte (dashed box) with vasculature labeled via rhodamine-dextran (magenta). Right panels track a single GFP+ monocyte (arrow). Note that the microglia respond to laser ablation while the monocyte remains in the vasculature. (**b**) Microglia (green) and vasculature (magenta) before and 15 minutes after laser ablation (core). (**c**) Change in mean rhodamine fluorescence showing a significant decrease, rather than increase, over time around the vessels or in the parenchyma following ablation, suggesting that rhodamine does not enter the brain and that the blood brain barrier is intact (n=16 mice, one-way repeated measures ANOVA, $p=0.023$, $F(11,15)=3.98$). Graph shows mean±SEM (magenta) and individual animals (gray). See Supplementary Table 1 for the number of females and males used in these experiments.

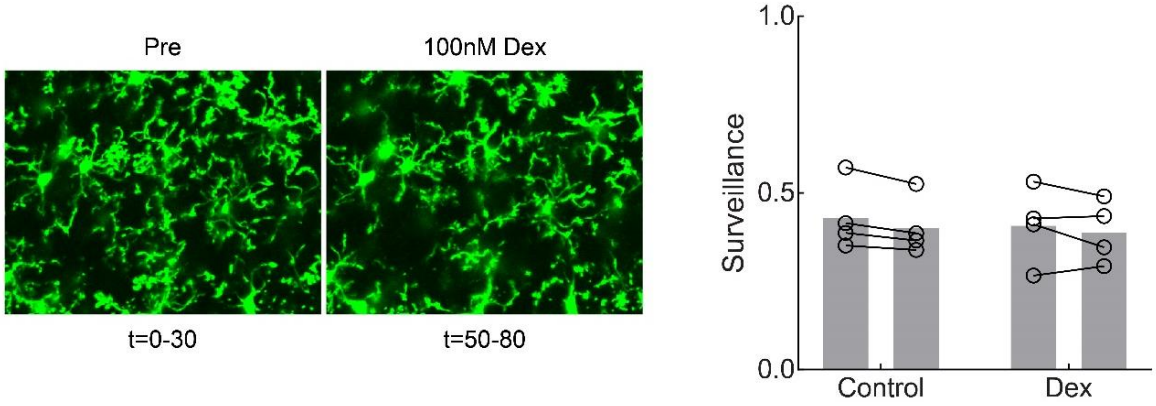

Supplementary Figure 4| Dexmedetomidine does not affect microglial surveillance in acute cortical slices. Microglial morphology was imaged for 30 minutes before either vehicle or dexmedetomidine (DEX) were applied. A second 30 minute imaging session was then acquired after a 20 minute infusion period. Left panel: Representative images showing microglial surveillance before (pre) and after (post) 100 nM DEX treatment. Right panel: Quantification of the surveillance ratio from control (vehicle-treated) and DEX-treated slices, pre and post treatment. . No significant differences were found between treatment (n=4 mice for both groups, two-way RM- ANOVA, no significant main effects for treatment ($p=0.80$, $F(1,6)=0.070$), or time ($p=0.088$, $F(1,6)=4.17$), or interaction ($p=0.70$, $F(1,6)=0.17$)). Graphs show mean±SEM. Points represent individual animals. See Supplementary Table 1 for the number of females and males used in these experiments.

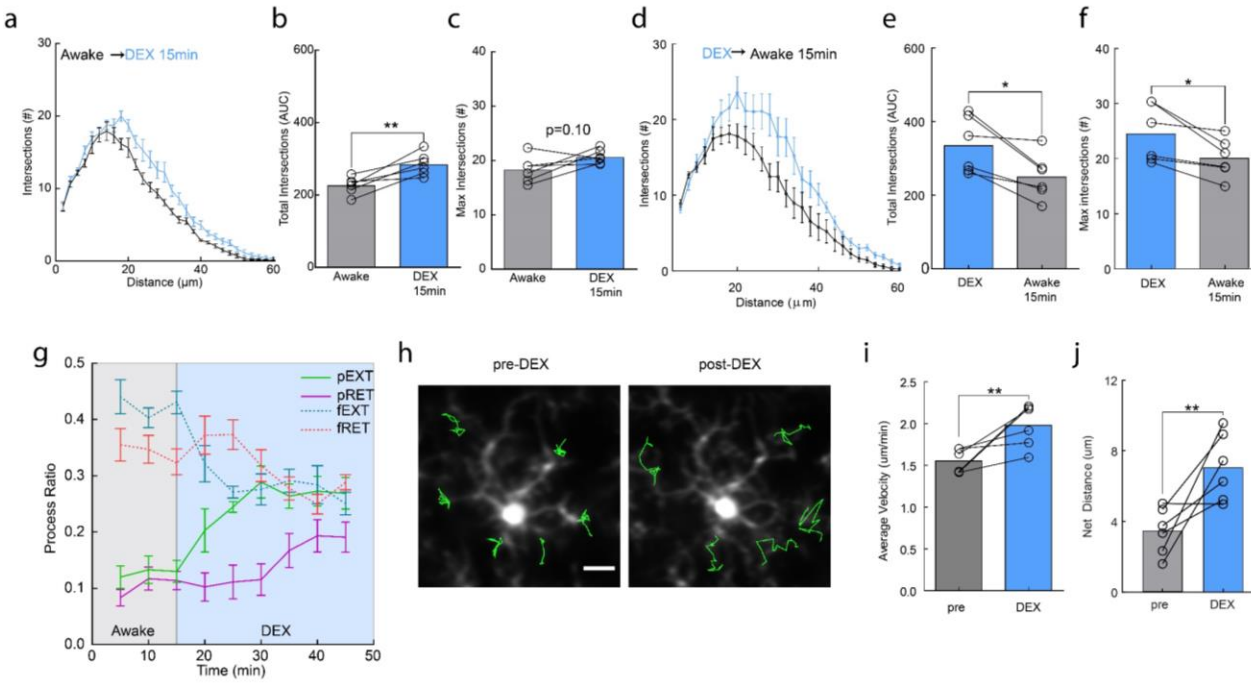

Supplementary Figure 5| Dexmedetomidine produces rapid and reversible effects on microglial morphology and process dynamics through changes to filopodia and pseudopodia formation. (**a**) Sholl profile of microglia imaged while first awake and then 15 minutes after dexmedetomidine (DEX) administration(n=6 mice, 3-5 microglia per mouse). Note that the same microglia assayed before and after DEX show an increase in arbor complexity quantified using the Sholl (**b**) area under the curve (AUC) (n=6 mice, two-sided paired t-test, P=0.0085, t(5)=4.19) and (**c**) maximum number of process intersections which shows a trend towards an increase (n=6 mice, two-sided paired t-test, p=0.10, t(5)=1.99). (**d**) DEX anesthesia is rapidly reversible with the administration of atipamezole. The Sholl profile of microglia 15 minutes after the administration of atipamezole is greatly reduced (n=6 mice 3-5 microglia per mouse), as quantified using (**e**) the AUC of the Sholl profile (n=6 mice, two-sided paired t-test, p=0.0151, t(5)=3.63) and (**f**) the maximum number of intersections (n=6 mice, two-sided paired t-test, p=0.0241, t(5)=3.20). (**g**) DEX rapidly (within 10 minutes of i.p. administration) causes a loss of filopodia and an increase in pseudopodia in the microglial process arbor (**h**) Example of a single microglia before and after DEX administration with process movements tracked in green. (**i**) The average velocity of microglial process increases after DEX anesthesia (n=6 mice, two-sided paired t-test, p=0.021, t(5)=3.33). (**j**) The net distance traveled by individual processes also increases after DEX anesthesia (n=6 mice, two-sided paired t-test, p=0.022, t(5)=3.30). Scale bar = 20μm. Graphs show mean±SEM; Abbreviations: pEXT=pseudopodia extension, pRET=pseudopodia retraction, fEXT=filopodia extension, fRET=filopodia retraction. *p<0.05, **p<0.01. Points represent individual animals. See Supplementary Table 1 for the number of females and males used in these experiments.

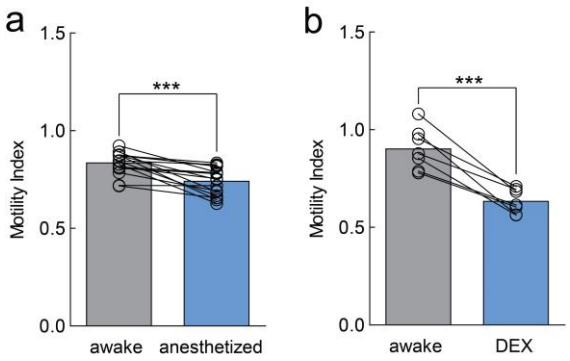

Supplementary Figure 6|Anesthesia decreases microglial motility. (**a**) Using a whole field motility index quantification which compares the gain and loss of pixels across 5-minute intervals, microglial motility in the field of view is globally decreased by fentanyl anesthesia (n=16 mice, two-sided paired t-test, p=0.00013, t(15)=5.09). (**b**) DEX alone also decreases microglial motility (n=7 mice, two-sided paired t-test p=0.00047, t(6)=6.87). Graphs show mean±SEM. Points represent individual animals. See Supplementary Table 1 for the number of females and males used in these experiments.

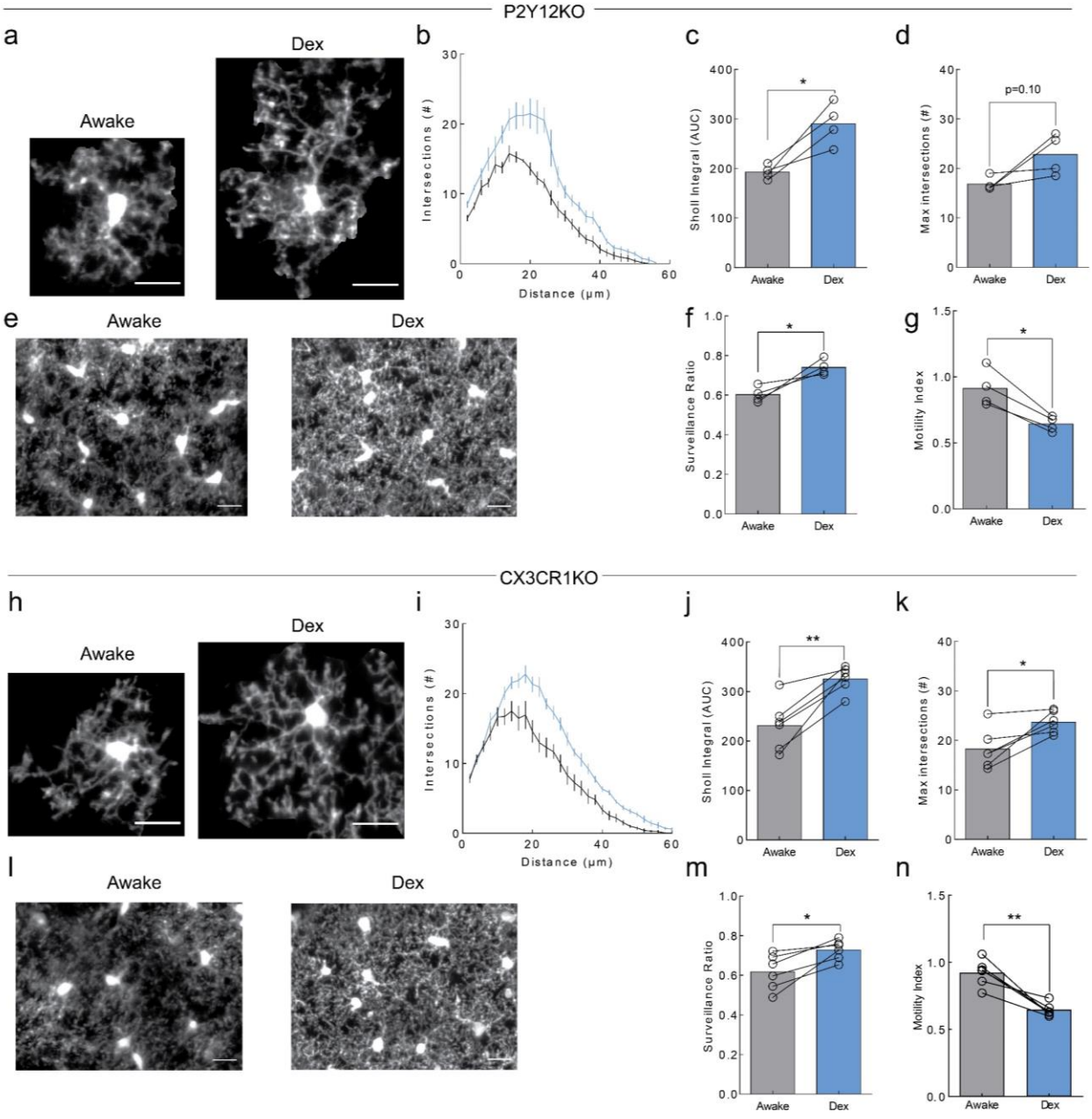

Supplementary Figure 7|P2Y12R and CX3CR1 are not responsible for the changes in microglial physiology between awake and anesthetized states. (**a**) Example microglial morphologies for awake and DEX anesthetized P2Y12KO animals. (**b**) Sholl analysis demonstrating a robust increase of intersections with DEX anesthesia in P2Y12KO animals (n=4 mice, 3-5 microglia per mouse). (**c**) Area under curve (AUC) quantification showing a significant increase in overall arbor complexity (n=4 mice, two-sided paired t-test, p=0.0223, t(3)=4.36). (**d**) The maximum number of intersections showed a trend towards increasing with DEX anesthesia in P2Y12KO animals (n=4 mice, two-sided paired t-test, P=0.10, t(3)=2.33). (**e**) Example 2D max-projection images of surveillance over a 1 hour period for awake and DEX anesthetized P2Y12KO mice. (**f**) Surveillance ratio significantly increased with DEX anesthesia in P2Y12KO mice (n=4 mice, two-sided paired t-test, p=0.038, t(3)=3.56). (**g**) The motility index was also reduced in DEX

anesthetized P2Y12KO mice (n=4 mice, two-sided paired t-test, p=0.011, t(3)=5.68). (**h**) Example microglial morphologies for awake and DEX anesthetized CX3CR1KO animals. (**i**) Sholl analysis demonstrating a robust increase in the number of intersections with DEX anesthesia in CX3CR1KO animals (n=6 mice, 3-5 microglia per mouse). (**j**) AUC quantification showing a significant increase in overall arbor complexity (n=6 mice, two-sided paired t-test, p=0.0030, t(5)=5.37). (**k**) The maximum number of intersections were also significantly increased with DEX anesthesia in CX3CR1KO animals (n=6 mice, two-sided paired t-test, p=0.017, t(5)=3.54). (**l**) Example 2D max-projection images of surveillance over a 1 hour period for awake and DEX anesthetized CX3CR1KO mice. (**m**) The surveillance ratio significantly increased with DEX anesthesia in CX3CR1KO mice (n=6 mice, two-sided paired t-test, p=0.012, t(5)=3.84). (**n**) The motility index was also reduced in DEX anesthetized CX3CR1KO mice (n=6 mice, two-sided paired t-test, p=0.0021, t(5)=5.81). Scale bars = 20μm. Graphs show mean±SEM. Points represent individual animals. See Supplementary Table 1 for the number of females and males used in these experiments.

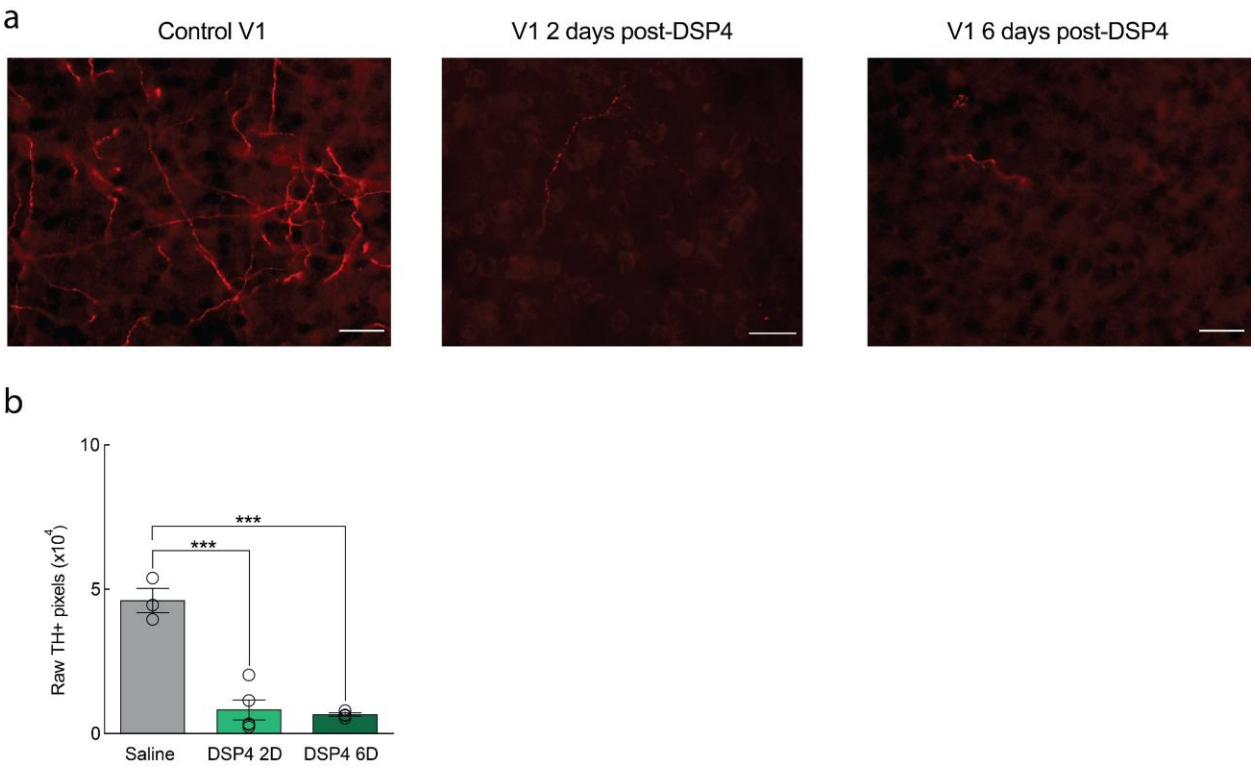

Supplementary Figure 8|DSP4 robustly and rapidly ablates noradrenergic projections in the visual cortex. (**a**) Example sections of visual cortex stained for TH fibers. DSP-4 causes a robust depletion of noradrenergic fibers at 2 and 6 days post-injection. (**b**) Quantification of total TH+ pixels showing significant depletion after DSP4 administration (n: S=3, DSP4 2D=5, DSP4 6D=4 treated mice, one-way ANOVA, $p=2.4x10^{-5}$, $F(2,9)=43.25$, Holm-Sidak multiple comparisons, S v. 2D $p=4.8x10^{-5}$, S v. 6D $p=4.8x10^{-5}$). Scale bars = 25μm. Graphs show mean±SEM. Abbreviations: S=saline, DSP4=N-(2-Chloroethyl)-N-ethyl-2-bromobenzylamine, 2D=2 days post-dose, 6D=6 days post-dose; *p<0.05, **p<0.01, ***p<0.005. Points represent individual animals. See Supplementary Table 1 for the number of females and males used in these experiments.

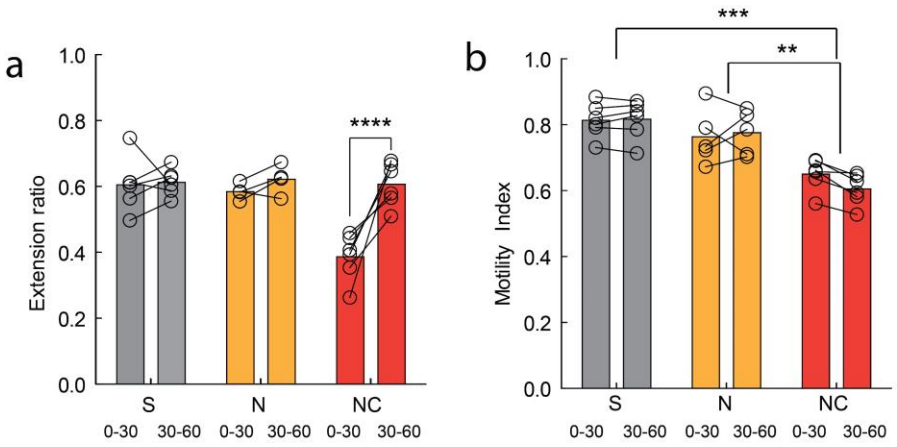

Supplementary Figure 9| Clenbuterol rapidly reduces microglia pseudopodia extension and motility. (**a**) In addition to the decrease in pseudopodia extension observed in clenbuterol-treated (NC) mice, we see a concomitant transient loss of pseudopodia extension (n: S=6, N=5, NC=6 mice, two-way repeated measures ANOVA, main effect of treatment (p=0.00084, F(2,13)=12.82), time (p=0.0018, F(1,13)=15.27) and interaction (p=0.0026, F(2,13)=9.72), Holm-Sidak multiple comparisons, NC 0-30 v. 30-60, p=0.00012). (**b**) NC treated microglia have reduced process motility for the duration of imaging (n: S=6, N=5, NC=6 mice, two-way RM-ANOVA, significant main effect of treatment (p=0.00013, F(2,14)=18.11), Holm-Sidak multiple comparisons: S v. NC, p=0.00014, N v. NC, p=0.0018). Graphs show mean±SEM. Abbreviations: S=saline, N=nadolol, NC=nadolol/clenbuterol; *p<0.05, **p<0.01, ***p<0.005, ****p<0.0001. Points represent individual animals. See Supplementary Table 1 for the number of females and males used in these experiments.

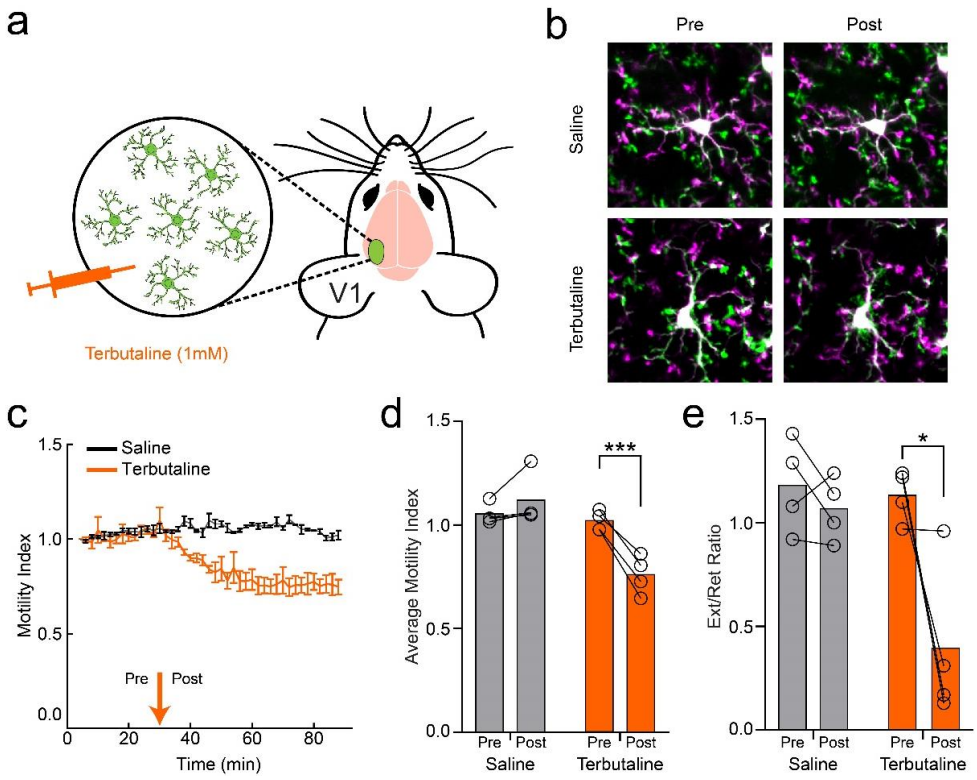

Supplementary Figure 10| Direct terbutaline application reduces motility and pseudopodia extension in microglia. (**a**) Schematic of experimental setup. The β2-AR agonist, terbutaline (1mM), was applied directly to microglia (green) through an open cranial window in the visual cortex (V1) of mice anesthetized with the fentanyl cocktail. (**b**) Example images of microglia before and after in either saline administered controls (top) or terbutaline administered animals (bottom). Time lapse overlays correspond to the first 30 minutes of baseline, and the first 30 minutes following injection where extension (green), retraction (magenta), and stable areas (white) are represented. Note the decreased number of pseudopodia following terbutaline administration. (**c**) Motility index plotted as a function of time for the baseline period (time before orange arrow, pre), and after injection (time after orange arrow, post) of saline (black) or terbutaline (orange) treated animals. (**d**) Quantification of the average motility index during the Pre period (0-30min) and the end of the Post period (60-90min) with saline and terbutaline treatment showing a decrease in motility index after terbutaline (n=4 mice, two-way RM-ANOVA, significant main effects of treatment ($p=0.01$, $F(1,6)=12.51$) and time ($p=0.0078$, $F(1,6)=15.33$) and interaction ($p=0.00060$, $F(1,6)=43.09$), Holm-Sidak multiple comparisons: terbutaline pre v. post, $p=0.00014$) (**e**) Quantification of the total number of extension pseudopodia divided by the number of retraction pseudopodia (Ext/Ret Ratio) showed no difference post saline (gray) treatment, but a significant reduction in pseudopodia extension post terbutaline (orange) treatment (n=4 mice, two-way RM-ANOVA, significant main effects of treatment ($p=0.013$, $F(1,6)=11.96$) and time ($p=0.021$, $F(1,6)=9.57$); Holm-Sidak multiple comparisons: terbutaline pre v. post, $p=0.018$). A ratio of 1.0 represents approximately equal number of extension and retraction pseudopodia. Graphs show mean±SEM. *$p<0.05$, ***$p<0.005$. Points represent individual animals. See Supplementary Table 1 for the number of females and males used in these experiments.

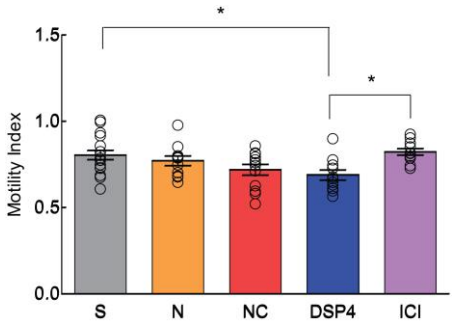

Supplementary Figure 11| In anesthetized adolescent mice NE depletion reduces motility. Microglial motility is reduced in DSP4-dosed mice (n: S=16, N=8, NC=12, DSP4=12, ICI =11 mice, one-way ANOVA, p=0.0061, F(4,57)=4.02), Holm-Sidak's multiple comparisons tests, S v. DSP4 p=0.029, DSP4 v. ICI p=0.020). Graphs show mean±SEM. Abbreviations: S=saline, N=nadolol, NC=nadolol/clenbuterol, DSP4=N-(2-Chloroethyl)-N-ethyl-2-bromobenzylamine; *p<0.05, ****p<0.0001. Points represent individual animals. See Supplementary Table 1 for the number of females and males used in these experiments.

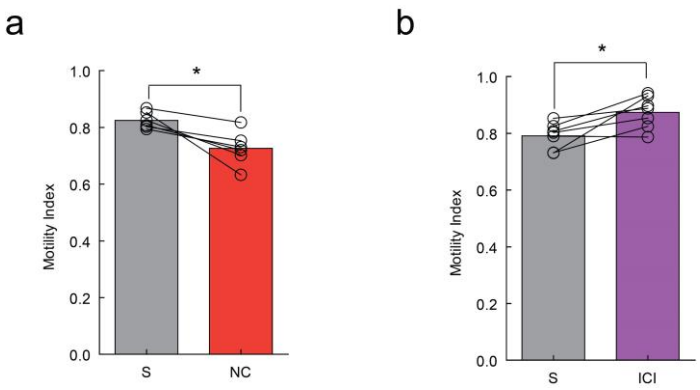

Supplementary Figure 12| In awake mice, β_2AR antagonism increases motility while agonism reduces motility. (**a**) In awake mice clenbuterol (NC) reduces microglial motility (n=6 mice, two-sided paired t-test, p=0.014, t(5)=3.71). (**b**) Microglial process motility is increased in ICI-dosed awake mice (n=7 mice, two-sided paired t-test, p=0.016, t(6)=3.34). Graphs show mean±SEM. Abbreviations: S=saline, NC=nadolol/clenbuterol, ICI=ICI-118,551; Points represent individual animals. See Supplementary Table 1 for the number of females and males used in these experiments.

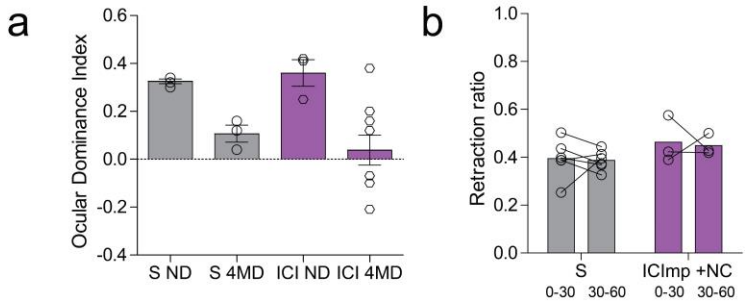

Supplementary Figure 13| ICI-118,551 does not alter ocular dominance plasticity. (**a**) Quantification of ocular dominance indices demonstrates robust shifts in saline (S) and ICI-118,551 treated groups (n: S ND=3, S 4MD=3, ICI ND=3, ICI 4MD=9 mice, two-way ANOVA, p=0.48, F(1,15)=0.51). (**b**) Imaging assay to confirm efficacy of mini-osmotic pump administration of ICI-118,551. ICI118, 551 given for 24hrs by mini-osmotic pump prevents microglial retraction elicited by clenbuterol *in vivo* (n: S=6, ICI = 3 mice, two-way RM-ANOVA, interaction p=0.93, F(1,7)=0.0080). Graphs show mean±SEM. Abbreviations: S=saline, ICI=ICI 118,551; ND=non-deprived, 4MD=4 days monocular deprivation. Points represent individual animals. See Supplementary Table 1 for the number of females and males used in these experiments.

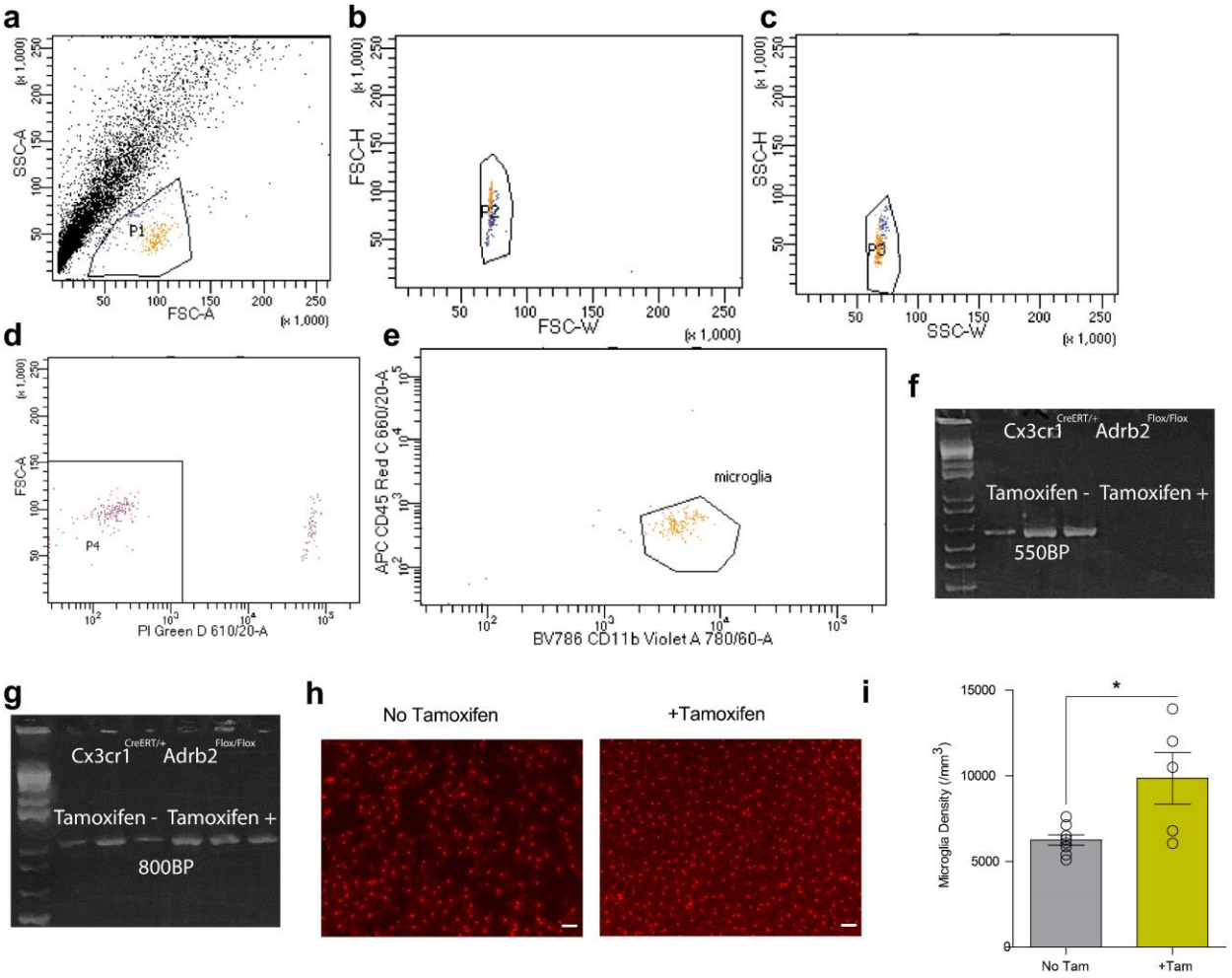

Supplementary Figure 14| CX3CR1-Cre^{ERT} successfully drives excision of β_2ARs in microglia. (**a-e**) Example FACS for microglia, microglia were sorted as PI negative (live), CD45^{lo}, and CD11b^{Hi}. (**f**) PCR for the presence of the β_2AR floxed allele. In mice given tamoxifen the allele is no longer present, suggesting excision (3 replicates per condition, replicates are individual animals, the experiment was repeated 3 times with similar outcomes). (**g**) PCR for the presence of the floxed excision product. Recombination occurs in both the untreated and tamoxifen-treated mice due to leakiness of the Cre in this line (3 replicates per condition, replicates are individual animals, the experiment was repeated 3 times with similar outcomes). (**h**) There is a significant degree of tdTomato expression in the visual cortex in CX3CR1-Cre/$\beta_2$flx/Ai9 mice which have not received tamoxifen treatment. (**i**) Comparison of the density of Tdtomato positive microglia in the visual cortex in CX3CR1-Cre/$\beta_2$flx/Ai9 mice with and without tamoxifen administration (n: No Tam=8, Tam=5 mice, two-sided student's t-test, p=0.013, t(11)=2.96). Scale bars = 50μm. Graphs show mean±SEM. Points represent individual animals. See Supplementary Table 1 for the number of females and males used in these experiments.

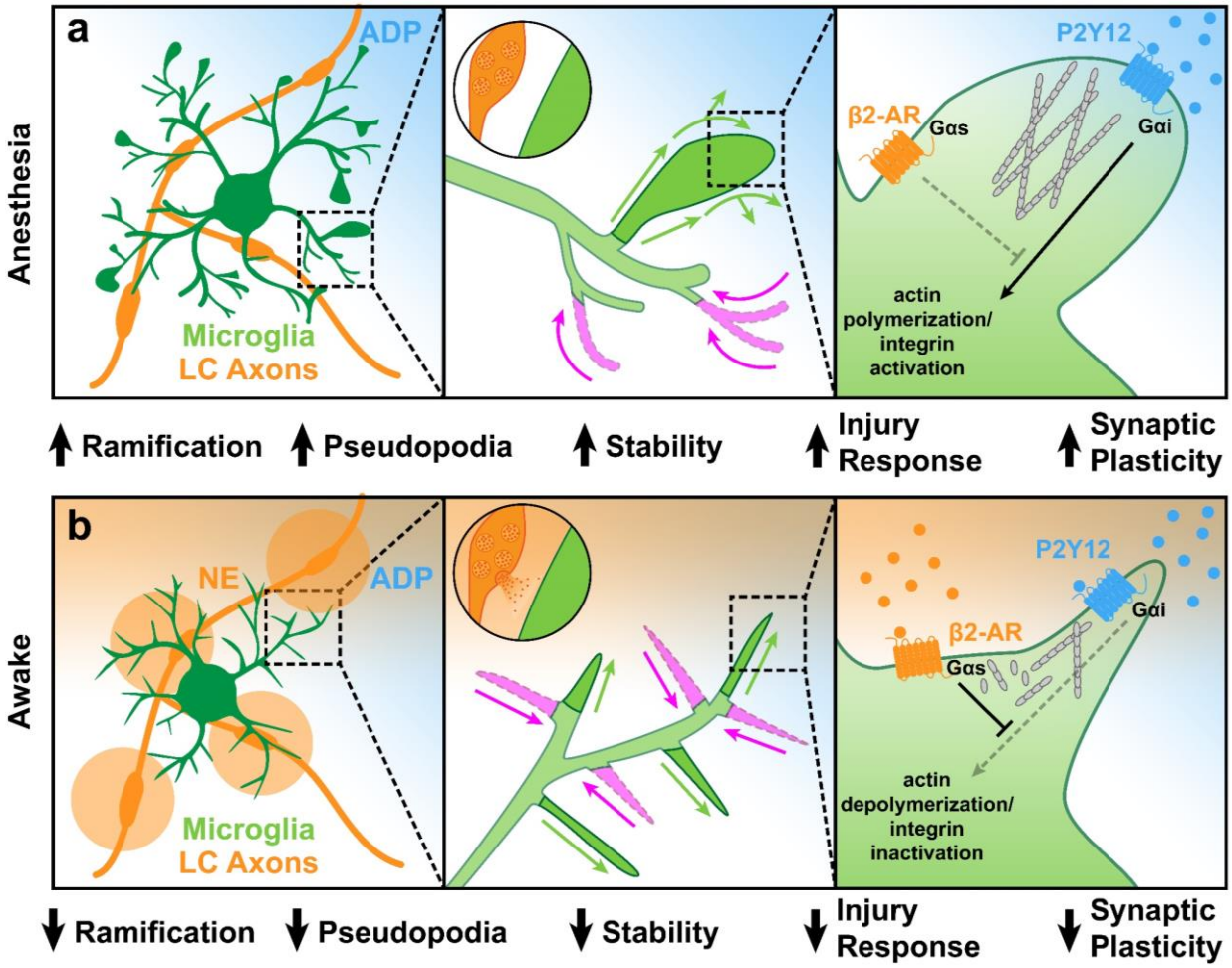

Supplementary Figure 15| Summary model of results. (**a**) Microglial dynamics during anesthesia. Left panel: during anesthesia microglia (green) extend secondary and tertiary processes to adopt a more ramified state when cortical NE release from locus coeruleus axons (orange) is low. Larger pseudopodia extend and remain stable. Middle panel: microglial motility decreases as processes extend (green arrows) and filopodia retract (magenta). Pseudopodia formation increases towards chemokinetic factors such as ADP, increasing microglial responses to injury and facilitating microglial roles in synaptic plasticity. Right panel: Gαi-coupled signaling (such as from P2Y12) activates integrins and facilitates actin polymerization within extending pseudopodia. (**b**) Microglial dynamics during wakeful states. Left panel: during wakeful states, cortical NE release from LC (orange) causes microglial secondary and tertiary processes (green) to retract reducing microglial process ramification and reducing the formation of pseudopodia. Middle panel: microglial motility increases as processes retract and filopodia quickly extend (green) and retract (magenta). Right panel: Gαi-coupled signaling is attenuated by NE via Gαs-coupled β2-ARs resulting in integrin deactivation and actin depolymerization. Subsequently, microglial responses to injury and roles in synaptic plasticity are inhibited.